Catalysis Science & Technology

ROYAL SOCIETY OF CHEMISTRY

PAPER

View Article Online
View Journal | View Issue

Cite this: *Catal. Sci. Technol.*, 2024, **14**, 1666

Cerium modification enhances the performance of Pd/USY for formaldehyde catalytic oxidation at room temperature†

Xiaofeng Liu, [ab] Chunying Wang,[ac] Yaobin Li, *[ace] Jingyi Wang,[abc] Xudong Chen[abc] and Hong He *[abcd]

Received 16th October 2023,
Accepted 6th February 2024

DOI: 10.1039/d3cy01436c

rsc.li/catalysis

Pd–Ce/USY catalysts were prepared by an impregnation method and then tested for their performance in formaldehyde (HCHO) catalytic oxidation at room temperature after H_2 reduction activation. We observed that Ce doping had a dramatic promotion effect on the Pd/USY catalysts. The Pd–Ce/USY catalyst with a loading of 0.5 wt% Pd and 0.5 wt% Ce exhibited a HCHO conversion of 80% with a WHSV of 300 000 mL g^{-1} h^{-1} and a HCHO inlet concentration of 150 ppm at 25 °C. Multiple physicochemical characterization tests were performed to investigate the mechanism of the Ce-promotion effect. The results illustrated that the Pd dispersion was increased due to the interaction between the CeO_2 and Pd nanoparticles over the 0.5Pd–0.5Ce/USY-R catalyst. The increase in Pd dispersion enhanced the number of hydrogen spillover sites during the H_2 reduction activation process, which induced more oxygen vacancies on the surface of the 0.5Pd–0.5Ce/USY-R catalyst. In addition, abundant oxygen vacancies were also formed owing to the increased ratio of Ce^{3+} on the 0.5Pd–0.5Ce/USY-R catalyst, which facilitated the activation of surface OH groups and surface-active oxygen species. Therefore, the HCHO oxidation performance and stability of the 0.5Pd–0.5Ce/USY-R catalyst was improved.

1. Introduction

Formaldehyde (HCHO), which is considered a priority indoor air pollutant, is released from wood-based materials, flooring materials, insulation materials, coatings and so on.[1] Long-term exposure to HCHO (even at ppm levels) will be harmful to the eyes, skin, and respiratory system, and can even cause cancer.[1,2] In order to meet strict environmental regulations and ensure public health, numerous strategies have been developed to eliminate HCHO from indoor air, for instance, adsorption,[3] photocatalytic oxidation,[4] thermal catalytic oxidation,[5] photo-thermal catalytic oxidation,[6] and plasma technology.[7] For adsorption, as well known, because of their limited adsorption ability, adsorbents need frequent regeneration. For photocatalytic oxidation, plasma technology, and high-temperature thermal catalytic oxidation, additional equipment such as light sources, plasma devices, or heating devices are required, increasing the application cost and inducing secondary pollutants such as ozone. Among various methods, room-temperature catalytic oxidation is the most promising, with many outstanding advantages such as energy efficiency, low operating temperature and lack of harmful by-products. Noble metal (Pt, Pd, Ir, Rh) catalysts are widely used due to their excellent HCHO catalytic activity at room temperature.[8–11]

Surface oxygen vacancies (OVs) are believed to be favourable for room-temperature HCHO oxidation on noble metal catalysts. Liu *et al.*[12] proposed that oxygen atoms in O_2 and HCHO are first trapped on the oxygen vacancies over Pt/$NaInO_2$, which facilitates the subsequent HCHO oxidation reaction. Oxygen vacancies are important active sites for water dissociation to form surface hydroxyl groups to directly transform surface formate into final products.[13] Higher concentrations of oxygen vacancies were found to better activate O_2 and improve the mobility of oxygen, thereby enhancing the catalytic activity of Au/CeO_2 catalysts.[14] In

[a] *Center for Excellence in Regional Atmospheric Environment, Key Laboratory of Urban Pollutant Conversion, Institute of Urban Environment, Chinese Academy of Sciences, Xiamen 361021, China. E-mail: ybli@iue.ac.cn*
[b] *University of Chinese Academy of Sciences, Beijing 100049, China*
[c] *Zhejiang Key Laboratory of Urban Environmental Processes and Pollution Control, CAS Haixi Industrial Technology Innovation Center in Beilun, Ningbo 315800, China*
[d] *State Key Joint Laboratory of Environment Simulation and Pollution Control, Research Center for Eco-environmental Sciences, Chinese Academy of Sciences, Beijing, 100085, China. E-mail: honghe@rcees.ac.cn*
[e] *Xiamen Key Laboratory of Materials for Gaseous Pollutant Control, Institute of Urban Environment, Chinese Academy of Sciences, Xiamen 361021, China*
† Electronic supplementary information (ESI) available. See DOI: https://doi.org/10.1039/d3cy01436c

addition, the oxygen vacancies of Pd/CeO_2 are conducive to adsorbing oxygen species. These oxygen species could adsorb the HCHO molecule and oxidize it immediately to dioxymethylene (DOM).[15]

Several strategies have been used to enhance the concentration of oxygen vacancies, including metal doping,[14,16,17] organic solvent addition,[18] high-temperature hydrogen reduction,[9,13] $NaBH_4$ reduction,[19,20] shape control,[21] and so on. Ceria could enhance the catalytic activity *via* the metal–support interaction and/or improved dispersion of the active metal component.[22–24] In addition, ceria has been shown to possess excellent oxygen storage capacity (OSC).[25] Previous studies found that oxygen vacancies can be produced by the transformation between Ce^{3+} and Ce^{4+} ($4Ce^{4+} + O^{2-} \rightarrow 2Ce^{4+} + 2Ce^{3+} + \square + 0.5O_2$ ($\square$ represents an empty position)) over ceria-based materials.[26] The higher the relative concentration of Ce^{3+}, the more oxygen vacancies can be formed.[27]

In our previous study, an acid treatment strategy was found to improve the hydroxyl concentration and further enhance the performance of Pd/USY catalysts in HCHO catalytic oxidation.[28] In the present work, an appropriate amount of Ce was introduced into the Pd/USY catalyst to further improve the catalytic activity, and the effect of Ce addition on Pd/USY catalysts was also investigated. It was found that Ce doping had a dramatic promotion effect on the Pd/USY catalyst. The 0.5Pd–0.5Ce/USY-R catalyst showed much higher performance for HCHO oxidation than the corresponding Ce-free catalyst, achieving 80% conversion of 150 ppm of HCHO to CO_2 and H_2O at a weight hourly space velocity (WHSV) of 300 000 mL g^{-1} h^{-1} at 25 °C. The catalysts were then characterized by a variety of techniques. Based on the characterization results, the effects of Ce doping were discussed and elucidated.

2. Experimental section

2.1 Catalyst preparation and characterization

Details of the preparation and characterization of the catalysts are described in the ESI.†

2.2 Activity test

The experimental conditions for the activity testing of the catalysts for HCHO catalytic oxidation were according to our previous work,[29] but the WHSV was controlled at 300 000 mL g^{-1} h^{-1}.

3. Results and discussion

3.1 HCHO catalytic activity

Fig. 1 and S1† show the catalytic activity of the fresh and reduced catalysts for HCHO oxidation. As shown in Fig. S1a,† the fresh catalysts possessed the ability of HCHO removal only at the beginning of the activity test, and there was no CO_2 yield (shown in Fig. S1b†), which means that the removal of HCHO was due to adsorption. A similar phenomenon was observed on the USY-R and 0.5Ce/USY-R samples as shown in Fig. 1, indicating that the removal of HCHO by the supports and Pd^{2+} species can be excluded. In contrast, the activities of the 0.5Pd/USY-R and 0.5Pd–0.5Ce/USY-R catalysts were greatly enhanced compared to the fresh catalysts after loading with Pd particles followed by reduction treatment, indicating that metallic Pd species were the main active sites for HCHO oxidation. It is worth noting that at the beginning of the testing, the HCHO conversion rates of 0.5Pd/USY-R and 0.5Pd–0.5Ce/USY-R were 80% and 90%, respectively. After 12 hours of testing, the HCHO conversion rate on 0.5Pd/USY-R decreased to 53%, while on 0.5Pd–0.5Ce/USY-R, the HCHO conversion rate maintained at 80%. Meanwhile, from Fig. S2,† the CO_2 yield rates and HCHO conversion rates showed the same trend over the 0.5Pd/USY-

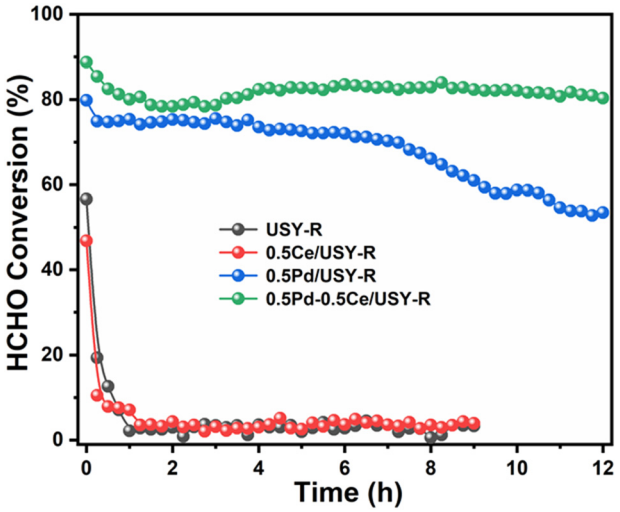

Fig. 1 HCHO conversion over USY-R, 0.5Ce/USY-R, 0.5Pd/USY-R and 0.5Pd–0.5Ce/USY-R catalysts. Reaction conditions: HCHO 150 ppm, 20 vol% O_2, 35% RH, He balance, WHSV 300000 mL g^{-1} h^{-1} at 25 °C.

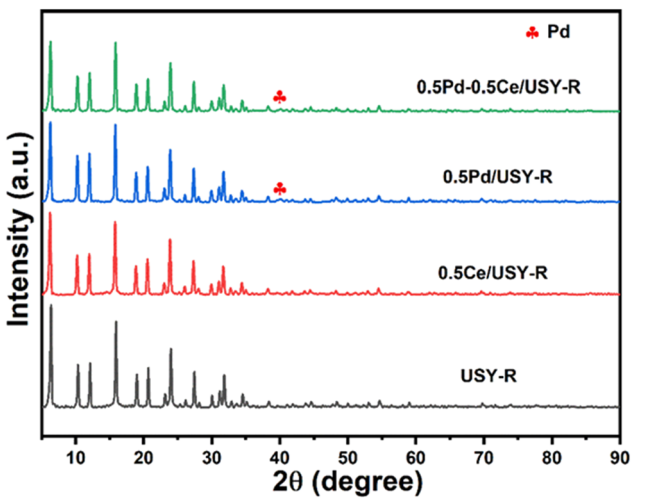

Fig. 2 XRD patterns of USY-R, 0.5Ce/USY-R, 0.5Pd/USY-R and 0.5Pd–0.5Ce/USY-R catalysts.

Table 1 Specific surface area (S_{BET}), Pd particle size (D) and Pd dispersion (d) of USY-R, 0.5Ce/USY-R, 0.5Pd/USY-R and 0.5Pd–0.5Ce/USY-R catalysts

Catalysts	S_{BET} (m^2 g^{-1})	D^a (nm)	d^b (%)
0.5Pd–0.5Ce/USY-R	688.4	5.82	19.3
0.5Pd/USY-R	667.5	7.12	15.8
0.5Ce/USY-R	662.2	—	
USY-R	686.4	—	

[a] Pd particle size measured with HAADF-STEM. [b] Pd dispersion calculated based on D.[10]

R and 0.5Pd–0.5Ce/USY-R catalysts. From Fig. S3,† the 0.5Pd–0.5Ce/USY-R catalyst exhibited excellent stability and with approximately 63% HCHO conversion for a 50 h-long test. It is clear that Ce doping on the carriers not only significantly improved the catalytic activity of the 0.5Pd–0.5Ce/USY-R catalyst for HCHO oxidation but also greatly enhanced its stability.

3.2 Structure of catalysts

XRD patterns of the reduced catalysts are shown in Fig. 2. No diffraction peaks for ceria can be observed in any of the XRD patterns, indicating that the ceria nanoparticles were uniformly dispersed and very small in size. One diffraction peak at 40.1° appeared in the patterns of the 0.5Pd/USY-R and 0.5Pd–0.5Ce/USY-R catalysts, which was assigned to Pd species. The results indicated that Pd particles were introduced on the catalysts.

Table 1 summarizes the BET surface areas of the four catalysts. The USY-R, 0.5Ce/USY-R, 0.5Pd/USY-R and 0.5Pd–0.5Ce/USY-R catalysts possessed similar specific surface areas of 686.4, 662.2, 667.5 and 688.4 m^2 g^{-1}, respectively. Fig. S4† shows the nitrogen adsorption–desorption isotherms of the USY-R, 0.5Ce/USY-R, 0.5Pd/USY-R and 0.5Pd–0.5Ce/USY-R catalysts. All catalysts showed type I hysteresis loops, indicating that the catalysts possessed a large number of micropores.

Fig. 3 and Table 1 show the HAADF-STEM images and Pd nanoparticle size distributions of 0.5Pd/USY-R and 0.5Pd–0.5Ce/USY-R. Interestingly, the Pd size distributions of 0.5Pd–0.5Ce/USY-R was clearly smaller than that of 0.5Pd/USY-R, which might be related to the formation of a Pd–CeO_2 interaction on 0.5Pd–0.5Ce/USY-R during the loading of Pd.

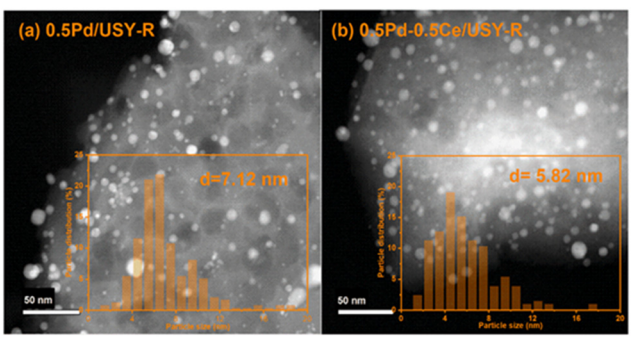

Fig. 3 HAADF-STEM images and particle size distributions of 0.5Pd/USY-R and 0.5Pd–0.5Ce/USY-R catalysts.

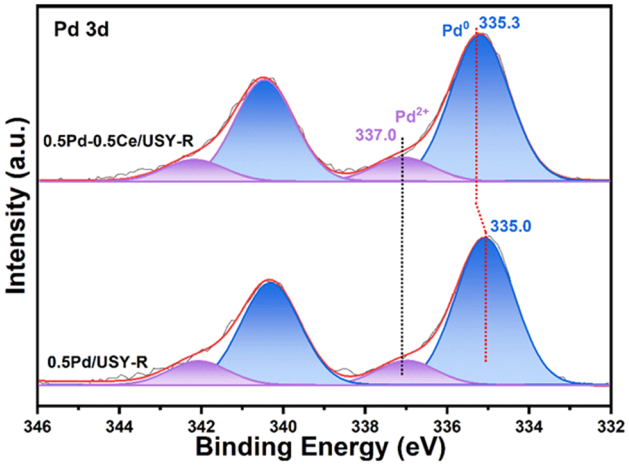

Fig. 4 Pd 3d XPS spectra of 0.5Ce/USY-R and 0.5Pd–0.5Ce/USY-R catalysts.

3.3 Chemical states of catalysts

Fig. 4 shows the Pd 3d XPS spectra of the 0.5Pd/USY-R and 0.5Pd–0.5Ce/USY-R catalysts. Two kinds of Pd species were observed on both catalysts. The peak at 337.0 eV was ascribed to PdO, which may be attributed to the re-oxidation of metal Pd particles in air during the transfer of the sample to the XPS chamber.[30,31] The peak at 335.3 eV of the 0.5Pd/USY-R catalyst and 335.0 eV of the 0.5Pd–0.5Ce/USY-R catalyst can be ascribed to metallic Pd.[32] It can be observed that a shift of Pd 3d to a higher binding energy occurred on the 0.5Pd–0.5Ce/USY-R catalyst, indicating the presence of a strong Pd–CeO_2 interaction.[33]

Fig. 5 and Table S1† show the Ce 3d XPS spectra of the 0.5Ce/USY-R and 0.5Pd–0.5Ce/USY-R catalysts. The

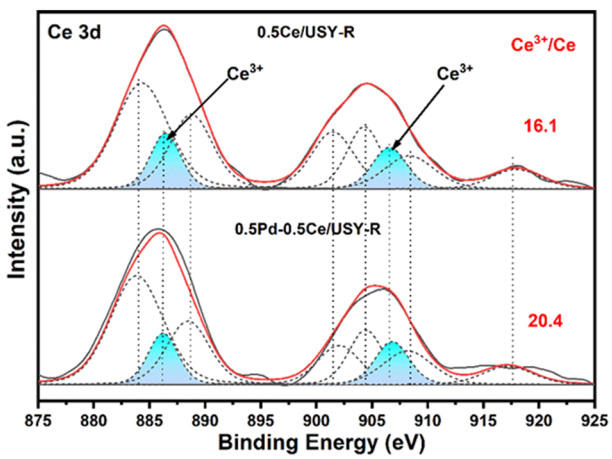

Fig. 5 Ce 3d XPS spectra of 0.5Ce/USY-R and 0.5Pd–0.5Ce/USY-R catalysts.

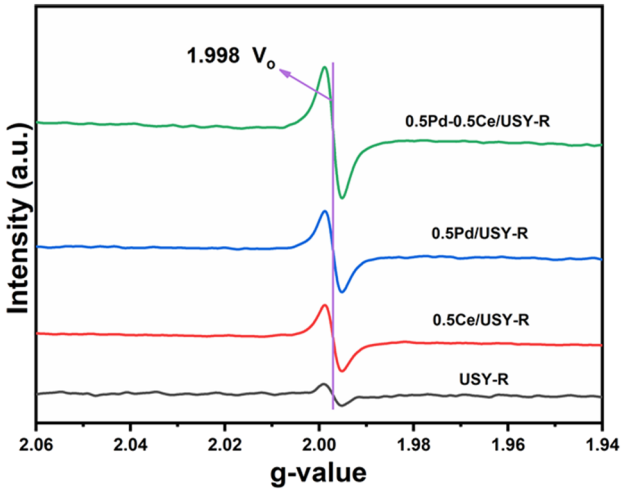

Fig. 6 ESR of USY-R, 0.5Ce/USY-R, 0.5Pd/USY-R and 0.5Pd–0.5Ce/USY-R catalysts.

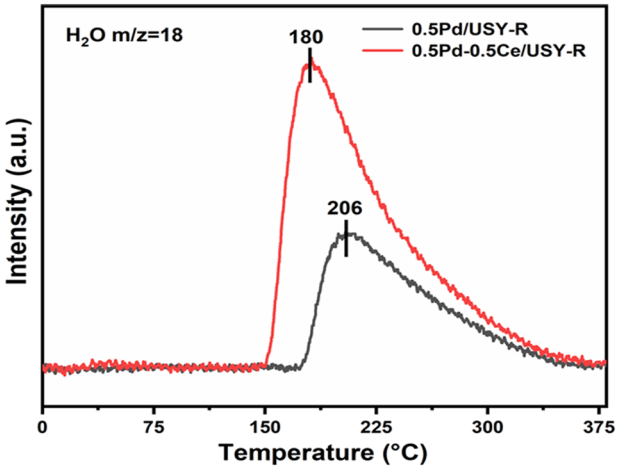

Fig. 7 H_2-TPSR profiles of 0.5Pd/USY-R and 0.5Pd–0.5Ce/USY-R catalysts.

concentration of Ce^{3+} on the 0.5Pd–0.5Ce/USY-R catalyst was higher than that on the 0.5Ce/USY-R catalyst, indicating that there were more oxygen vacancies on the 0.5Pd–0.5Ce/USY-R catalyst.[27]

3.4 Defect analysis

ESR was further used to examine the oxygen vacancies present in the catalysts and the results are shown in Fig. 6. All the samples showed a signal at g = 1.998, which was ascribed to oxygen vacancies.[34] Notably, the USY-R catalysts possessed the weakest signal intensity, which was ascribed to the formation of framework oxygen vacancies during acid treatment. After doping Ce on the USY support, the signal intensity became stronger for the 0.5Ce/USY-R catalyst, which implied that Ce doping could produce oxygen vacancies on the Ce-USY sample. According to previous studies, oxygen vacancies can be produced by the transformation between Ce^{3+} and Ce^{4+}, $4Ce^{4+} + O^{2-} \rightarrow 2Ce^{4+} + 2Ce^{3+} + \square + 0.5O_2$ ($\square$ represents an empty position) over ceria-based materials.[26,27] Ce^{4+} could be reduced to Ce^{3+} during the hydrogen reduction treatment. The Ce 3d XPS results were in line with the results of ESR. After loading Pd on the 0.5Ce/USY support, the signal intensity was greatly enhanced on the 0.5Pd–0.5Ce/USY-R catalyst, which was attributed to hydrogen spillover during high-temperature hydrogen reduction.[9]

3.5 Surface-active oxygen species

H_2-TPSR measurements were used to investigate the activation of surface O species on the reduced catalysts, according to the following reaction occurred during the H_2-TPSR process: $2H_2 + O_2 \rightarrow 2H_2O$, and the results are shown in Fig. 7. The influence of the adsorbed H_2O has been excluded (Fig. S5†). As shown in Fig. 7, broad H_2O desorption peaks at 206 °C and 180 °C were observed in the range of 0–375 °C over the 0.5Pd/USY-R and 0.5Pd–0.5Ce/USY-R catalysts, respectively. Compared to the 0.5Pd/USY-R catalyst, the 0.5Pd–0.5Ce/USY-R catalyst exhibited a larger H_2O desorption peak area, indicating that the catalyst consumed more active O_2 to form H_2O. In addition, the H_2O desorption peak temperature for the 0.5Pd–0.5Ce/USY-R catalyst was lower than that of the 0.5Pd/USY-R catalyst, implying that the activity of the active O_2 was stronger. It is clear that after doping with Ce, the 0.5Pd–0.5Ce/USY-R catalyst possessed more surface-active oxygen species than the 0.5Pd/USY-R catalyst, and the surface-active oxygen species were more reactive. Surface-active oxygen species play significant roles in the HCHO oxidation reaction.[35,36] Therefore, the activity of HCHO oxidation on the 0.5Pd–0.5Ce/USY-R catalyst was significantly enhanced by Ce doping.

The CO-TPR experiment was carried out to determine whether the activation of the surface OH species was enhanced on the Ce-doped 0.5Pd/USY catalyst, according to the reaction mechanism $2CO + 2OH \rightarrow 2CO_2 + H_2$,[37] and

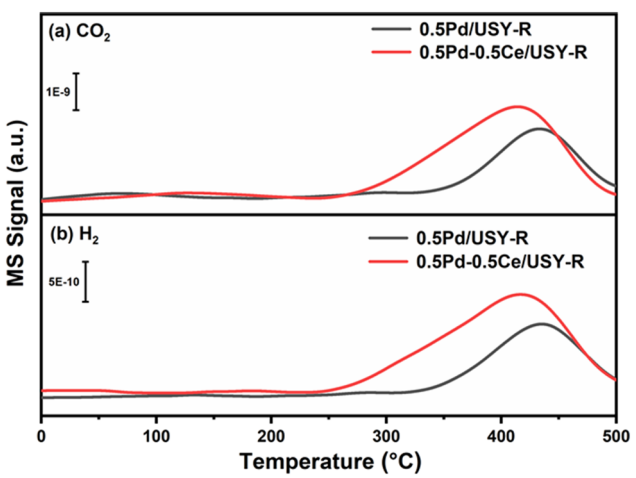

Fig. 8 CO-TPR profiles (a) CO_2 and (b) H_2 on 0.5Pd/USY-R and 0.5Pd–0.5Ce/USY-R catalysts.

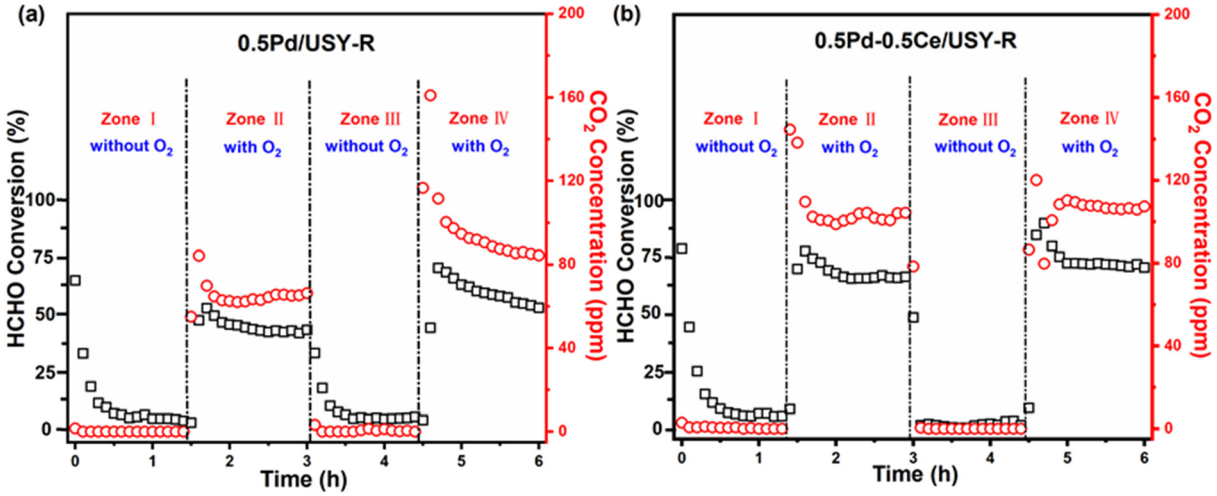

Fig. 9 O_2 effects on the activity of (a) 0.5Pd/USY-R and (b) 0.5Pd–0.5Ce/USY-R catalysts. Reaction conditions: 150 ppm of HCHO, 20% O_2, 35% RH, He balance, 400 000 mL g^{-1} h^{-1} WHSV, 25 °C.

the results are shown in Fig. 8. Smaller amounts of CO_2 and H_2 were produced on the 0.5Pd/USY-R catalyst without Ce doping, which indicated that there were fewer OH groups on the 0.5Pd/USY-R catalyst. In contrast, larger amounts of CO_2 and H_2 were observed on the 0.5Pd–0.5Ce/USY-R catalyst in the range of 0–500 °C, suggesting that abundant OH groups existed on the 0.5Pd–0.5Ce/USY-R surface. Previous studies have reported that surface OH groups could be produced with the oxygen vacancies on CeO_2.[38,39] Therefore, the increased in the number of surface OH on the 0.5Pd–0.5Ce/USY-R catalyst can be attributed to the increase in oxygen vacancies after Ce doping. The surface OH groups play an important role in HCHO catalytic oxidation;[40] thus, the enhancement of the surface OH concentration by Ce doping is one of the main reasons for the improved performance of 0.5Pd–0.5Ce/USY-R for HCHO oxidation.

3.6 Role of H_2O in HCHO oxidation

O_2 and H_2O startup–shutdown cycling experiments were carried out next to clarify the role of O_2 and H_2O in HCHO oxidation, and the results are shown in Fig. 9 and 10. As shown in Fig. 9, there was a similar phenomenon on the 0.5Pd/USY-R and 0.5Pd–0.5Ce/USY-R catalysts. When the gas flow has no O_2, the catalysts showed almost no activity for HCHO oxidation (zones I and III); however, HCHO conversion was achieved after introducing O_2 into the gas flow (zones II and IV). As shown in Fig. 10, the HCHO conversion of the 0.5Ce/USY-R and 0.5Pd–0.5Ce/USY-R catalysts depended on the presence of moisture. When there was no moisture in the gas flow, the HCHO conversion gradually decreases with the prolongation of test time (zones I and III). After introducing water vapor into the gas flow, the HCHO conversion was significantly enhanced (zones II and IV).

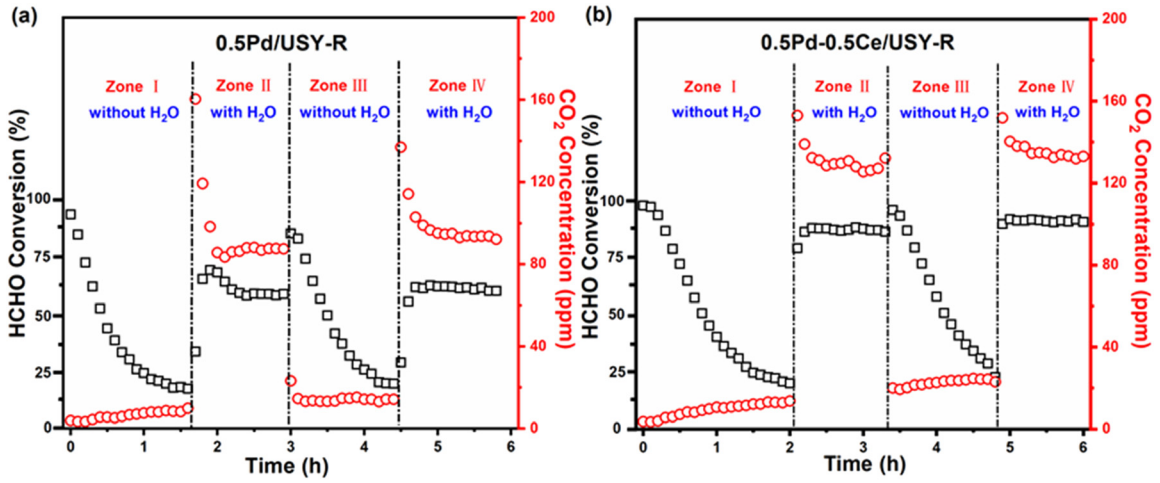

Fig. 10 H_2O effects on the activity of (a) 0.5Pd/USY-R and (b) 0.5Pd–0.5Ce/USY-R catalysts. Reaction conditions: 150 ppm of HCHO, 20% O_2, 35% RH, He balance, 400 000 mL g^{-1} h^{-1} WHSV, 25 °C.

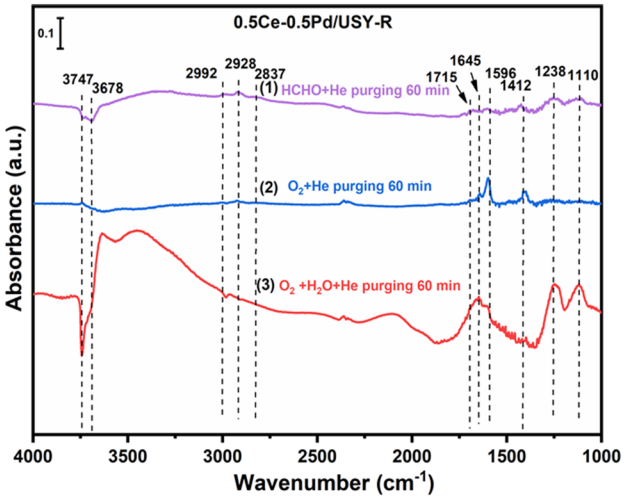

Fig. 11 *In situ* DRIFTS spectra over 0.5Ce–0.5Pd/USY-R in a flow of HCHO + He for 60 min (1); followed by O_2 + He purging for 60 min (2); O_2 + H_2O + He purging for 60 min (3) at room temperature. Reaction conditions: 150 ppm of HCHO, 20% O_2, 35% RH, He balance, the total flow rate of 100 mL min^{-1}.

The above results indicated that there was a synergistic effect between H_2O and O_2 in HCHO oxidation on the 0.5Pd/USY-R and 0.5Pd–0.5Ce/USY-R catalysts at room temperature. Previous studies reported that surface OH groups are formed by water dissociation on oxygen vacancies or on metal surfaces through water–oxygen interactions,[41–44] which then enhanced the diffusion of oxygen.[45,46] Because the 0.5Pd–0.5Ce/USY-R catalyst possessed more oxygen vacancies than the 0.5Pd/USY-R catalyst, it had a much higher capacity for O_2 and H_2O activation, thus significantly enhancing the HCHO oxidation activity and stability.

3.7 Reaction mechanism

The reaction mechanism of HCHO oxidation on the 0.5Pd–0.5Ce/USY-R and 0.5Pd/USY-R catalysts was next investigated at room temperature using *in situ* DRIFTS. As shown in Fig. 11 and S7,† HCHO oxidation on the 0.5Pd–0.5Ce/USY-R and 0.5Pd/USY-R catalysts followed a similar reaction pathway. After being exposed to HCHO + He, the dioxymethylene (DOM) species (1110 and 1238 cm^{-1}), formate species (1412 and 1596 cm^{-1}),[40,47,48] adsorbed HCHO molecules (1715 cm^{-1}),[49] ν(C–H) (2837, 2928 and 2992 cm^{-1}), and surface hydroxyl species (3678 and 3747 cm^{-1})[50] were observed. Then, after the introduction of O_2, the adsorbed HCHO molecules were decreased. Finally, after introducing H_2O + O_2, the ν(OH) (band ranging from 3600 to 2800 cm^{-1}) and $\delta(H_2O)$ (1645 cm^{-1}) dramatically increased, and the bands at 1110 and 1238 cm^{-1} should also be assigned to adsorbed water (the USY-R support test is displayed in Fig. S6†). To summarize the above experimental phenomena, it was concluded that the HCHO oxidation over 0.5Ce–0.5Pd/USY-R and 0.5Pd/USY-R follows the two-step pathway: HCHO + OH → H_2CO_2(DOM) + OH → HCOO + OH → CO_2 + H_2O.

4. Conclusions

In summary, this work demonstrates that Ce doping has a dramatic promotion effect on Pd/USY catalysts for ambient HCHO oxidation. As shown above, adding Ce to the Pd/USY catalyst led to the formation of well-dispersed Pd species, which possessed more active sites for hydrogen spillover during the H_2 reduction activation process and induced more oxygen vacancies. Furthermore, due to the presence of Ce, oxygen vacancies were also produced by the transformation between Ce^{3+} and Ce^{4+} during hydrogen reduction treatment. More oxygen vacancies facilitated the activation of surface OH groups and surface-active oxygen species and thus significantly increased the catalytic activity and stability of the 0.5Pd–0.5Ce/USY catalyst for ambient HCHO destruction. In future work, a deeper exploration of the interaction mechanisms between noble metals and Ce species could be accomplished through theoretical calculations. This will elucidate the pivotal roles of various Ce states in HCHO oxidation. The theoretical and experimental foundations established by such investigations will contribute significantly to the development of cost-effective and efficient catalysts.

Author contributions

Xiaofeng Liu: investigation, writing – original draft, validation, and software. Chunying Wang: software, visualization, and writing – review & editing. Yaobin Li: conceptualization, supervision, writing – review & editing, and funding acquisition. Jingyi Wang: investigation. Xudong Chen: investigation. Hong He: supervision, review & editing, and funding acquisition.

Conflicts of interest

There are no conflicts to declare.

Acknowledgements

This work was supported by the National Key Research and Development Program of China (2022YFC3702802), the Youth Innovation Promotion Association, CAS (2020310), the Science and Technology Planning Project of Xiamen City (3502Z20191021), and the Science and Technology Innovation "2025" major program in Ningbo (2022Z028).

Notes and references

1 T. Salthammer, S. Mentese and R. Marutzky, *Chem. Rev.*, 2010, **110**, 2536–2572.
2 M. Hakim, Y. Broza, O. Barash, N. Peled, M. Phillips, A. Amann and H. Haick, *Chem. Rev.*, 2012, **112**, 5949–5966.
3 J. Yu, X. Li, Z. Xu and W. Xiao, *Environ. Sci. Technol.*, 2013, **47**, 9928–9933.
4 J. Yu, S. Wang, J. Low and W. Xiao, *Phys. Chem. Chem. Phys.*, 2013, **15**, 16883–16890.

5 C. Zhang, F. Liu, Y. Zhai, H. Ariga, N. Yi, Y. Liu, K. Asakura, M. Flytzani-Stephanopoulos and H. He, *Angew. Chem., Int. Ed.*, 2012, **51**, 9628–9632.
6 J. Xie, S. Wang and F. Wang, *Appl. Surf. Sci.*, 2024, **644**, 158709.
7 W. J. Liang, J. Li, J. X. Li, T. Zhu and Y. Q. Jin, *J. Hazard. Mater.*, 2010, **175**, 1090–1095.
8 J. Xie, S. Wang, K. Zhao, M. Wu and F. Wang, *Inorg. Chem.*, 2023, **62**, 904–915.
9 C. Wang, Y. Li, C. Zhang, X. Chen, C. Liu, W. Weng, W. Shan and H. He, *Appl. Catal., B*, 2021, **282**, 119540.
10 Y. Li, X. Chen, C. Wang, C. Zhang and H. He, *ACS Catal.*, 2018, **8**, 11377–11385.
11 X. Sun, J. Lin, H. Guan, L. Li, L. Sun, Y. Wang, S. Miao, Y. Su and X. Wang, *Appl. Catal., B*, 2018, **226**, 575–584.
12 F. Liu, J. Shen, D. Xu, W. Zhou, S. Zhang and L. Wan, *Chem. Eng. J.*, 2018, **334**, 2283–2292.
13 Y. Li, C. Zhang, J. Ma, M. Chen, H. Deng and H. He, *Appl. Catal., B*, 2017, **217**, 560–569.
14 G. Rochard, J. Giraudon, L. Liotta, V. Parola and J. Lamonier, *Catal. Sci. Technol.*, 2019, **9**, 3203–3213.
15 K. Li, J. Ji, H. Huang and M. He, *Chemosphere*, 2020, **246**, 125762.
16 L. Zhu, J. Wang, S. Rong, H. Wang and P. Zhang, *Appl. Catal., B*, 2017, **211**, 212–221.
17 S. Rong, K. Li, P. Zhang, F. Liu and J. Zhang, *Catal. Sci. Technol.*, 2018, **8**, 1799–1812.
18 R. Fang, H. Huang, J. Ji, M. He, Q. Feng, Y. Zhan and D. Leung, *Chem. Eng. J.*, 2018, **334**, 2050–2057.
19 M. He, J. Ji, B. Liu and H. Huang, *Appl. Surf. Sci.*, 2019, **473**, 934–942.
20 J. Ye, M. Zhou, Y. Le, B. Cheng and J. Yu, *Appl. Catal., B*, 2020, **267**, 118689.
21 S. Wang, Y. Wang and F. Wang, *Appl. Catal., A*, 2022, **630**, 118469.
22 D. Chen, H. Shen, Y. Zhang, X. Zou, A. Guan and Y. Wang, *Catal. Lett.*, 2022, **152**, 187–198.
23 X. Zhang and P. Shi, *J. Mol. Catal. A: Chem.*, 2003, **194**, 99–105.
24 M. Rønning, F. Huber, H. Meland, H. Venvik, D. Chen and A. Holmen, *Catal. Today*, 2005, **100**, 249–254.
25 J. Kašpar and P. Fornasiero, *J. Solid State Chem.*, 2003, **171**, 19–29.
26 X. Liu, K. Zhou, L. Wang, B. Wang and Y. Li, *J. Am. Chem. Soc.*, 2009, **131**, 3140–3141.
27 Y. Zhang, Y. Yu, W. Shan, Z. Lian and H. He, *Catal. Today*, 2020, **339**, 135–147.
28 X. Liu, C. Wang, Y. Chen, Q. Qin, Y. Li and H. He, *J. Environ. Sci.*, 2023, **125**, 811–822.
29 X. Liu, C. Wang, Y. Li and H. He, *Catal. Sci. Technol.*, 2022, **12**, 6540–6547.
30 X. Zhu, M. Shen, L. Lobban and R. Mallinson, *J. Catal.*, 2011, **278**, 123–132.
31 K. Otto, L. Haack and J. deVries, *Appl. Catal., B*, 1992, **1**, 1–12.
32 H. Yang, G. Zhang, X. Hong and Y. Zhu, *J. Mol. Catal. A: Chem.*, 2004, **210**, 143–148.
33 Y. Zhou, D. Liu, Z. Liu, L. Feng and J. Yang, *ACS Appl. Mater. Interfaces*, 2020, **12**, 47065–47075.
34 I. Hussain, A. Jalil, N. Hassan, H. Hambali and N. Jusoh, *Chem. Eng. Sci.*, 2020, **228**, 115978.
35 Y. Bu, Y. Chen, G. Jiang, X. Hou, S. Li and Z. Zhang, *Appl. Catal., B*, 2020, **260**, 118138.
36 J. Ye, Y. Yu, J. Fan, B. Cheng, J. Yu and W. Ho, *Environ. Sci.: Nano*, 2020, **7**, 3655–3709.
37 C. Wang, Y. Li, L. Zheng, C. Zhang, Y. Wang, W. Shan, F. Liu and H. He, *ACS Catal.*, 2020, **11**, 456–465.
38 H. Evin, G. Jacobs, J. Ruiz-Martinez, U. Graham, A. Dozier, G. Thomas and B. Davis, *Catal. Lett.*, 2008, **122**, 9–19.
39 H. Evin, G. Jacobs, J. Ruiz-Martinez, G. Thomas and B. Davis, *Catal. Lett.*, 2008, **120**, 166–178.
40 X. Chen, G. He, Y. Li, M. Chen, X. Qin, C. Zhang and H. He, *ACS Catal.*, 2020, **10**, 9706–9715.
41 Z. Zhang, O. Bondarchuk, B. Kay, J. White and Z. Dohna'lek, *J. Phys. Chem. B*, 2006, **110**, 21840–21845.
42 J. Vecchietti, A. Bonivardi, W. Xu, D. Stacchiola, J. Delgado, M. Calatayud and S. Collins, *ACS Catal.*, 2014, **4**, 2088–2096.
43 R. Ojifinni, N. Froemming, J. Gong, M. Pan, T. Kim, J. White, G. Henkelman and C. Mullins, *J. Am. Chem. Soc.*, 2008, **130**, 6801–6812.
44 J. G. Tae, S. Kim, R. A. Ojifinni, J. M. White and C. Buddie Mullins, *J. Am. Chem. Soc.*, 2006, **128**, 6282–6283.
45 L. Liu, B. McAllister, H. Ye and P. Hu, *J. Am. Chem. Soc.*, 2006, **128**, 4017–4022.
46 S. Ammal and A. Heyden, *ACS Catal.*, 2014, **4**, 3654–3662.
47 A. Tsyganenko and V. Filimonov, *Spectrosc. Lett.*, 1972, **5**, 477–487.
48 H. Lin, J. Long, Q. Gu, W. Zhang, R. Ruan, Z. Li and X. Wang, *Phys. Chem. Chem. Phys.*, 2012, **14**, 9468–9474.
49 H. Chen, M. Tang, Z. Rui and H. Ji, *Ind. Eng. Chem. Res.*, 2015, **54**, 8900–8907.
50 B. Bai and J. Li, *ACS Catal.*, 2014, **4**, 2753–2762.

